Available online at www.sciencedirect.com
SCIENCE DIRECT®
Physics and Chemistry of the Earth 29 (2004) 409–417
PHYSICS and CHEMISTRY of the EARTH
www.elsevier.com/locate/pce

Transfer function approach to signal discrimination of ULF geomagnetic data

M. Harada [a], K. Hattori [b,*], N. Isezaki [c]

[a] Graduate School of Science and Technology, Chiba University, 1-33, Yayoi, Inage, Chiba 263-8522, Japan
[b] Marine Biosystems Research Center, Chiba University, 1-33, Yayoi, Inage, Chiba 263-8522, Japan
[c] Department of Earth Sciences, Faculty of Science, Chiba University, 1-33, Yayoi, Inage, Chiba 263-8522, Japan
Available online 9 April 2004

Abstract

In order to study earthquake-related ULF geomagnetic field changes, it is important to discriminate the noises such as magnetic pulsations originated from solar–terrestrial interactions and artificial noises from DC-driven trains and factories. For this aim, the interstation transfer functions and wavelet transform method have been proposed and applied to the data obtained at the ULF electromagnetic sensor array at the Boso Peninsula, Japan. It is concluded that this interstation transfer function approach has a capacity for signal discrimination; that is, it shows effectiveness to eliminate noises originated from the external ionospheric sources and its secondary effects.

Keywords: ULF geomagnetic field changes; The interstation transfer functions; Wavelet transform; ULF electromagnetic sensor array; Signal discrimination

1. Introduction

Electromagnetic phenomena are recently considered as a promising candidate for the short-term prediction of large earthquakes. There have been accumulated observational reports in a very wide frequency range (e.g. Hayakawa and Fujinawa, 1994; Hayakawa, 1999; Hayakawa and Molchanov, 2002). Measurements of electromagnetic phenomena can be classified into three types; the passive ground-based observation, the ground-based observation with the use of transmitter signals, and the satellite observation. Among these observational methods, one of the most promising methods is the use of ULF emissions related with an earthquake, because convincing evidence of ULF magnetic signature of earthquakes has been reported (Fraser-Smith et al., 1990; Kopytenko et al., 1993; Molchanov et al., 1992; Hayakawa et al., 1996; Kawate et al., 1998; Hayakawa et al., 2000; Gotoh et al., 2002; Hattori et al., 2002). The advantage of this frequency range is the penetration of signals through the crust because of skin effect. The generation mechanisms of these electromagnetic phenomena have not been solved yet, though there have been proposed some mechanisms (Molchanov and Hayakawa, 1995; Vallianatos and Tzanis, 1999). In order to verify ULF electromagnetic phenomena preceding large earthquakes and to clarify the relationship between electromagnetic phenomena and possible generation mechanisms, we have installed sensitive geomagnetic sensors in Japan.

The observed ULF data consist of a few possible signals (see Fig. 1). The first one is the most intense, natural and global signals such as daily variation of the geomagnetic field and magnetic pulsations which are mainly originated from the external sources. The second one is artificial and regional noises which are generated by the underground current driven by a DC train and a factory. The last one is the more local signals around the magnetometer such as movement of magnetic objects, mechanical vibration of the ground, inner circuit noises. The signal associated with crustal activity is generally very weak, so that the problem is how to discriminate the earthquake-related signals from other noises. Several methods have already been proposed. Those are polarization analysis (Hayakawa et al., 1996; Hattori et al., 2002), fractal analysis (Hayakawa et al., 2000), and principal component analysis (Gotoh et al., 2002; Uyeda et al., 2002). In these papers, they mainly use data only

* Corresponding author. Tel.: +81-43-290-2801; fax: +81-43-290-2859.
E-mail address: hattori@earth.s.chiba-u.ac.jp (K. Hattori).

1474-7065/$ - see front matter © 2004 Elsevier Ltd. All rights reserved.
doi:10.1016/j.pce.2004.03.002

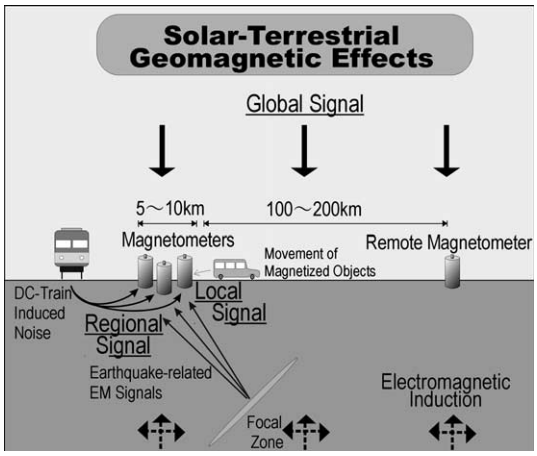

Fig. 1. Signals observed at a geomagnetic station array. The spatial feature of signals are as follows. (1) Global signals: simultaneous detection at remote stations which are located at a distance of more than hundred kms. (2) Regional signals: simultaneous detection at nearby stations which are distributed within a few tens kms. (3) Local signals: detection at only one station.

in the midnight time because the contamination of global natural signals and artificial noises is considered to be much less than those in daytime. We attempt in this paper to eliminate the noises of ULF geomagnetic variations by a combined use of the so-called interstation method (Beamish and Banks, 1983; Fujiwara and Toh, 1996) and wavelet transform (Morlet et al., 1982; Torrence and Compo, 1998). It was shown that global natural signals can be removed satisfactorily.

2. Formulation of signal discrimination

2.1. Interstation transfer function

It is well known that there exists a linear relation among the three components of geomagnetic field variations observed on the ground;

$$\Delta Z(\omega) = A(\omega)\cdot\Delta X(\omega) + B(\omega)\cdot\Delta Y(\omega), \tag{1}$$

where $\Delta X(\omega)$, $\Delta Y(\omega)$, and $\Delta Z(\omega)$ are geographic NS, EW, and vertical components of geomagnetic variations, respectively. These are mathematically complex Fourier components (Rikitake, 1969). This relation is interpreted as a linear system that has two inputs of $\Delta X(\omega)$ and $\Delta Y(\omega)$ and an output of $\Delta Z(\omega)$. The coefficients $A(\omega)$ and $B(\omega)$ are considered to be constants for a certain duration and specific to a given station, and are frequency-dependent complex transfer functions. The transfer functions are known to provide us with the information on the electric conductivity under the ground at the given station. So that, the transfer functions has been used to study the anomalies of the vertical field component.

We use, in this paper, the interstation method (Beamish and Banks, 1983; Fujiwara and Toh, 1996), and we also estimate horizontal transfer functions. Geomagnetic variations observed at a station can be separated into normal and anomalous parts. The normal part is mainly composed of an external field originated from ionospheric sources. On the other hand, the anomalous part is composed of only an internal field that arises from an induction current flowing in the "anomalous" earth structure; that is, the secondary magnetic fields due to the induction current at the lateral inhomogeneous structure (Beamish and Banks, 1983).

$$\begin{aligned}\begin{pmatrix}\Delta X_s(\omega)\\ \Delta Y_s(\omega)\\ \Delta Z_s(\omega)\end{pmatrix} &= \begin{pmatrix}\Delta X_n(\omega)\\ \Delta Y_n(\omega)\\ \Delta Z_n(\omega)\end{pmatrix} + \begin{pmatrix}\Delta X_a(\omega)\\ \Delta Y_a(\omega)\\ \Delta Z_a(\omega)\end{pmatrix}\\ &= \begin{pmatrix}\Delta X_n(\omega)\\ \Delta Y_n(\omega)\\ \Delta Z_n(\omega)\end{pmatrix} + \begin{pmatrix}C(\omega) & D(\omega) & G(\omega)\\ E(\omega) & F(\omega) & H(\omega)\\ A(\omega) & B(\omega) & I(\omega)\end{pmatrix}\\ &\quad\cdot\begin{pmatrix}\Delta X_n(\omega)\\ \Delta Y_n(\omega)\\ \Delta Z_n(\omega)\end{pmatrix} + \begin{pmatrix}\delta X(\omega)\\ \delta Y(\omega)\\ \delta Z(\omega)\end{pmatrix},\end{aligned} \tag{2}$$

where $A(\omega)$, $B(\omega)$, $C(\omega)$, $D(\omega)$, $E(\omega)$, $F(\omega)$, $G(\omega)$, $H(\omega)$, and $I(\omega)$ are interstation transfer functions and $\delta X(\omega)$, $\delta Y(\omega)$, and $\delta Z(\omega)$ are uncorrelated parts of the corresponding components including errors (Schmucker, 1970). Suffixes s, n, and a mean the signal observed at the site, signal originated from external sources, and that caused from the lateral heterogeneity under the ground, respectively. When the external electromagnetic wave penetrates into the ground vertically as a plane wave, $\Delta Z_n(\omega)$, $\delta X(\omega)$, $\delta Y(\omega)$, and $\delta Z(\omega)$ are negligibly small. Then, we get the following equation, where $\Delta X_r(\omega)$, $\Delta Y_r(\omega)$ are horizontal components of geomagnetic variations at the reference station.

$$\begin{aligned}\begin{pmatrix}\Delta X_s(\omega)\\ \Delta Y_s(\omega)\\ \Delta Z_s(\omega)\end{pmatrix} &= \begin{pmatrix}\Delta X_r(\omega)\\ \Delta Y_r(\omega)\\ 0\end{pmatrix} + \begin{pmatrix}C(\omega) & D(\omega)\\ E(\omega) & F(\omega)\\ A(\omega) & B(\omega)\end{pmatrix}\\ &\quad\cdot\begin{pmatrix}\Delta X_r(\omega)\\ \Delta Y_r(\omega)\end{pmatrix}\\ &= \begin{pmatrix}C(\omega)+1 & D(\omega)\\ E(\omega) & F(\omega)+1\\ A(\omega) & B(\omega)\end{pmatrix}\\ &\quad\cdot\begin{pmatrix}\Delta X_r(\omega)\\ \Delta Y_r(\omega)\end{pmatrix}.\end{aligned} \tag{3}$$

We use the data observed at the Kakioka Magnetic Observatory, Japan Meteorological Agency as the reference data in this study, because the Kakioka Magnetic Observatory is one of the most excellent observatories in the world. We rewrite Eq. (3) with the use of matrix $\mathbf{T}(\omega)$, $\mathbf{H}_s(\omega)$, and $\mathbf{H}_r(\omega)$ which are corresponding to the

interstation transfer function matrix, the data vectors at the site, and the reference site, respectively.

$$\mathbf{H}_s(\omega) = \mathbf{T}(\omega) \cdot \mathbf{H}_r(\omega), \tag{4}$$

or

$$\begin{pmatrix} H_{xs}(\omega) \\ H_{ys}(\omega) \\ H_{zs}(\omega) \end{pmatrix} = \begin{pmatrix} T_{xx}(\omega) & T_{xy}(\omega) \\ T_{yx}(\omega) & T_{yy}(\omega) \\ T_{zx}(\omega) & T_{zy}(\omega) \end{pmatrix} \cdot \begin{pmatrix} H_{xr}(\omega) \\ H_{yr}(\omega) \end{pmatrix}. \tag{4'}$$

2.2. Wavelet transform

The estimation of the transfer function is generally carried out by Fourier transform approach. In this paper we adopt the wavelet transform instead of FFT, because the artificial noises originated from a DC-driven train has a transient feature. The wavelet transform is useful in analyzing time series data which contain non-stationary power at many different frequencies. We adopt the Morlet wavelet (Morlet et al., 1982) to the interstation transfer function analysis because of its similarity to Fourier transform in this study. The Morlet wavelet is defined by $\psi_0(\eta)$ with sinusoidal function and Gaussian window as shown in Eq. (5).

$$\psi_0(\eta) = \pi^{-1/4} e^{i\beta\eta} e^{-\eta^2/2}, \tag{5}$$

where η is a non-dimensional time parameter. β is the non-dimensional frequency and here taken to be 6 to satisfy the admissibility condition (Farge, 1992). The continuous wavelet transform of a time series data x_n is defined as the convolution of x_n with a scaled and translated version of $\psi_0(\eta)$ as shown in Eq. (6).

$$W_n(s) = \sum_{n'=0}^{N-1} x_{n'} \psi^* \left[\frac{(n'-n)\delta t}{s} \right], \tag{6}$$

where $*$ indicates the complex conjugate. s and n are the wavelet scale and the localized time index n, respectively. The relation between wavelet scale s and Fourier frequency f is given as follows.

$$s = \left(\frac{\beta + \sqrt{2+\beta^2}}{4\pi} \right) \frac{1}{f}. \tag{7}$$

As for the reconstruction of the time series data, we use the sum of the real part of the wavelet transform over all scales (Farge, 1992),

$$x_n = \frac{\delta j \delta t^{1/2}}{C_\delta \psi_0(0)} \sum_{j=0}^{J} \frac{\mathrm{Re}\{W_n(s_j)\}}{s_j^{1/2}}. \tag{8}$$

The factor $\psi_0(0)$ removes the energy scaling, while the $s_j^{1/2}$ converts the wavelet transform to an energy density. $\psi_0(0)$ and C_δ are constant of $\pi^{-1/4}$ and 0.776 for our Morlet wavelet, respectively (Torrence and Compo, 1998).

2.3. Reduction of external source fields

After the interstation transfer functions are determined, we can estimate the possible external component at the observation site with use of the remote reference data. We obtain Eq. (9) in the wavelet domain instead of Eq. (4).

$$\mathbf{H}_{sn}^j = \mathbf{T}^j \cdot \mathbf{H}_r^j \tag{9}$$

The superscript j indicates the wavelet scale and $\mathbf{H}_{sn}$ is the reconstructed external signal at the observation site from the reference data. It means that $\mathbf{H}_{sn}$ includes only the global noise (natural signal) from the upper atmosphere associated with solar–terrestrial interaction. Therefore, if one subtracts the reconstructed data from the actually observed data at the site, it is expected that there are less global components in the residual of $\Delta\mathbf{H}^j$. It means the most intense component can be removed.

$$\Delta\mathbf{H}^j = \mathbf{H}_s^j - \mathbf{H}_{sn}^j. \tag{10}$$

3. Application to observed geomagnetic data

Fig. 2 shows the configuration map of the ULF geomagnetic stations in Japan. There are two geomagnetic sensor arrays with inter-sensor distance of about 5 km in the Boso and Izu Peninsulas. Both regions are located in one of the most active seismic zones in Japan. The Kakioka Magnetic Observatory, of which data are used as the remote reference data, is also shown in Fig. 2. The system time is synchronized by the GPS clock at each station. The original sampling rate is 50 Hz, but here we use the data resampled down to 1 Hz. In this

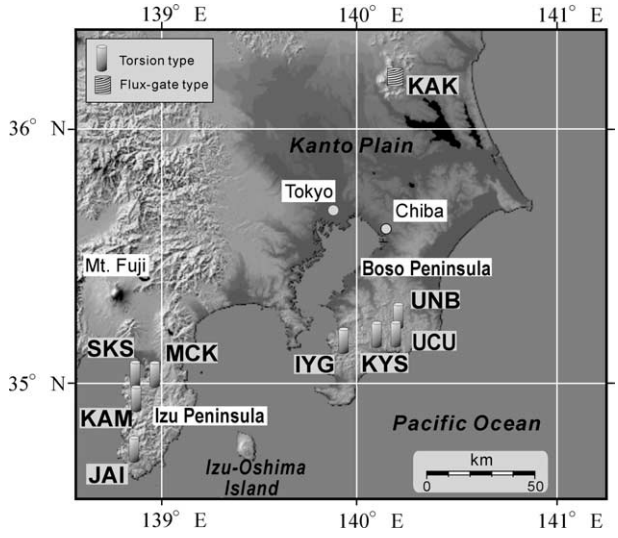

Fig. 2. The configuration map of geomagnetic stations. **KAK** indicates the Kakioka Magnetic Observatory, Japan Meteorological Agency. We use **KAK** data as a remote reference in computing interstation transfer functions of **UNB**, **UCU**, and **KYS** stations at Boso Peninsula.

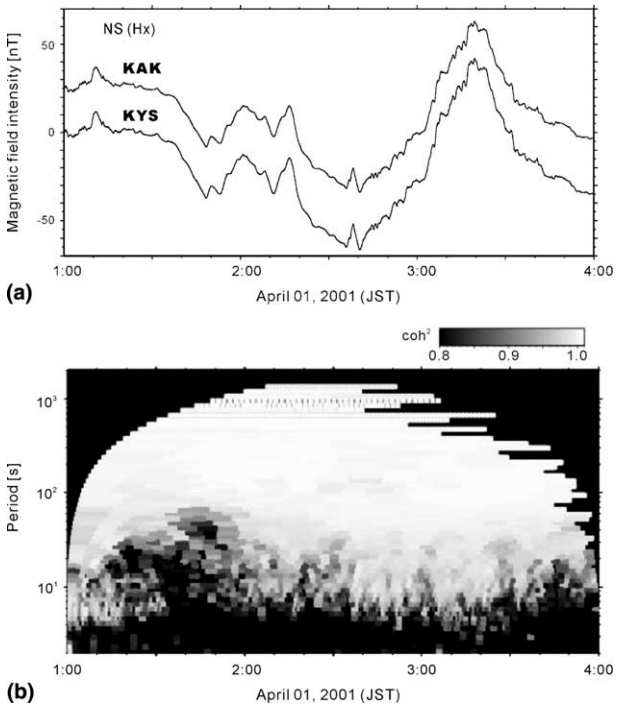

Fig. 3. The variations of the coherency between **KAK** and **KYS** (NS component) for an interval of 01:00–04:00 on April 1, 2001 when the geomagnetic activity is extremely high ($Kp = 8$). (a) The geomagnetic variations observed at **KAK** and **KYS**. (b) The time-frequency dependence of the squared coherences.

paper, we apply the proposed method to the data obtained at the stations in the Boso Peninsula. Fig. 3(a) shows the geomagnetic variation of NS component observed at **KAK** and **KYS** stations on April 1, 2001. Fig. 3(b) indicates the coherency between the two stations. In order to estimate the interstation transfer function (hereafter we call ISTF) between **KYS** and **KAK** stations, the midnight data (01:00–04:00, JST in the interval of January to April, 2001) with high correlation ($r \geqslant 0.9$) of the horizontal components are used. Fig. 4 shows the estimated ISTF between **KAK** and **KYS**. Open and solid circles indicate the real and imaginary part of ISTF, respectively, and solid and dashed lines indicate the upper and lower limit of standard deviation. The transfer function of periods more than 10 s in the horizontal components seem to be well estimated.

Fig. 5 shows the geomagnetic field variations observed at the array stations (**UNB**, **UCU**, and **KYS**) and Kakioka (**KAK**) in the 20 min interval of 04:24–04:44 (JST) on April 5, 2001. The trend variations of horizontal components, which are common for all stations, are global signals originated from the external source in the upper atmosphere. There exist the geomagnetic pulsations (04:35–04:38, $T \approx 12.5$ s), marked by arrows (1), which appeared simultaneously at all stations. While the changes detected only at the array stations (**UNB**, **UCU**, **KYS**), which are marked by an arrow (2), are considered to be regional noises generated by a DC-driven train. As for the vertical component, magnetic pulsation does not appear in the period of (1), and the tendency of the curve is different from each other. This implies that the vertical component of the external fields is quite small, and the assumption of $\Delta Z_n(\omega) = 0$ is not invalid.

Fig. 6(a) shows the NS component of geomagnetic field variations observed at **KAK** (1) and **KYS** (2) sta-

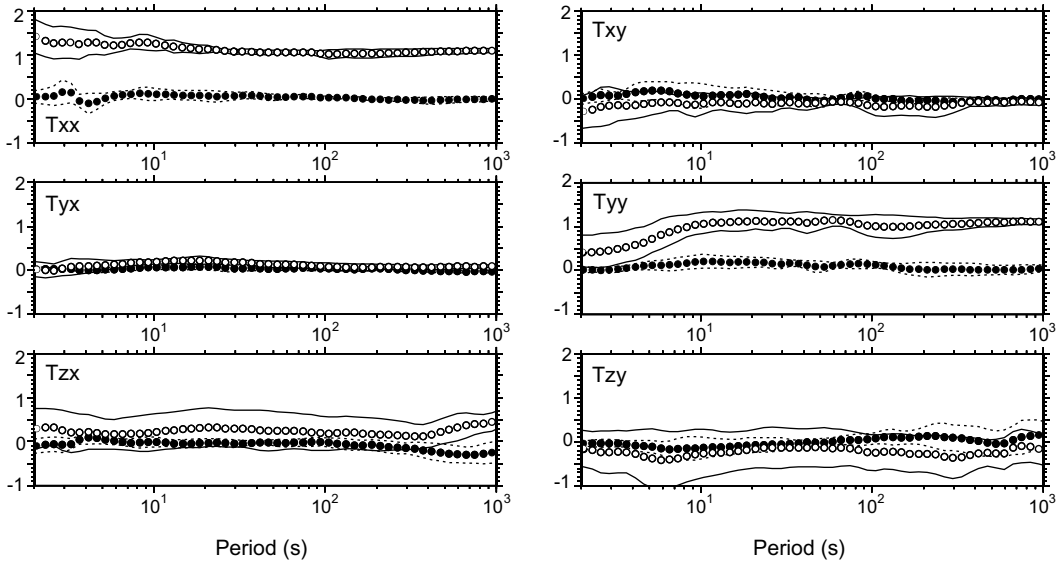

Fig. 4. The estimated interstation transfer functions between **KAK** and **KYS** stations. Open and solid circles indicate the real and imaginary part of ISTF, respectively. Solid and dashed lines indicate the real and imaginary part of the standard deviation of ISTF, respectively. ISTF are computed using midnight time data when a global intense external source exists.

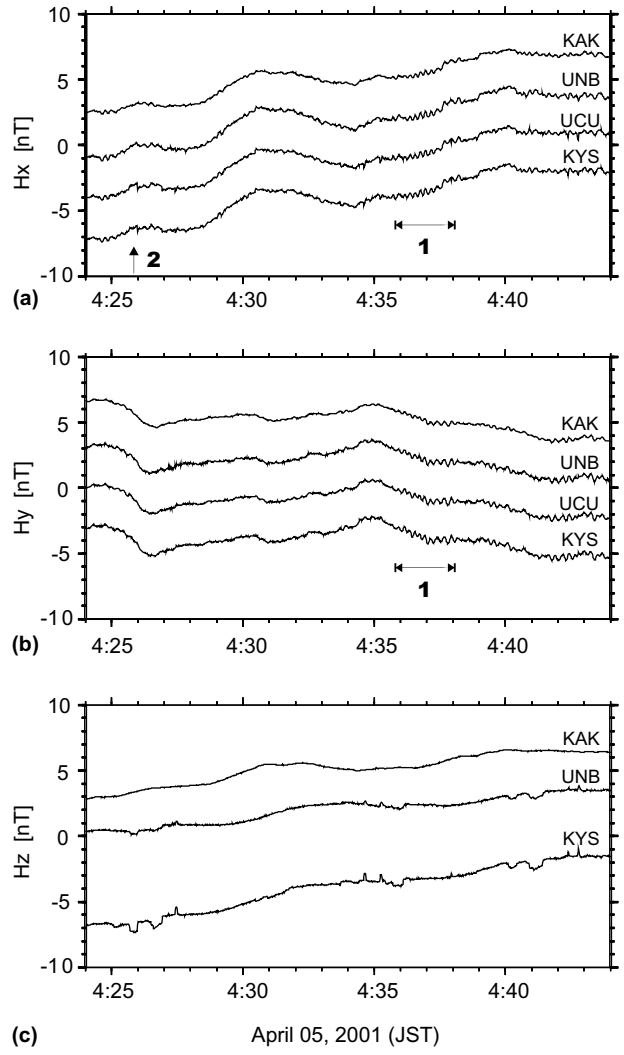

Fig. 5. Geomagnetic field variations observed for an interval of 04:24–04:44 on April 5, 2001(JST) at **UNB**, **UCU**, **KYS**, and **KAK** stations in Fig. 2. (a) North–South component (H_x). (b) East–West component (H_y). (c) Vertical component (H_z), (data missing at **UCU** in this interval). The arrows (1) indicate the time when the geomagnetic pulsations turned up. The arrow (2) indicates the regional artificial noise associated with DC-driven train around the array sites (**UNB**, **UCU** and **KYS**).

tions on April 5, 2001. Then Kp was 5+ and $\sum Kp$ was 25+. The apparent geomagnetic pulsation can be recognized after 04:35 in this figure. Fig. 6(b) is high pass filtered time-amplitude records ($T \leqslant 940$ s) at **KAK** (3), **KYS** (4), and the estimated variation obtained by the ISTF approach (5). Fig. 6(c) illustrates the residual between the observed and estimated values ((6) = (4)–(5)), which shows that the pulsation is nearly completely removed. Fig. 7 shows the global signal reduction at **KYS** for the term of 04:35–04:40, in which geomagnetic pulsations turned up at the same time both in **KAK** and array stations. It is safe to say that the magnetic pulsations have disappeared with the use of the presented

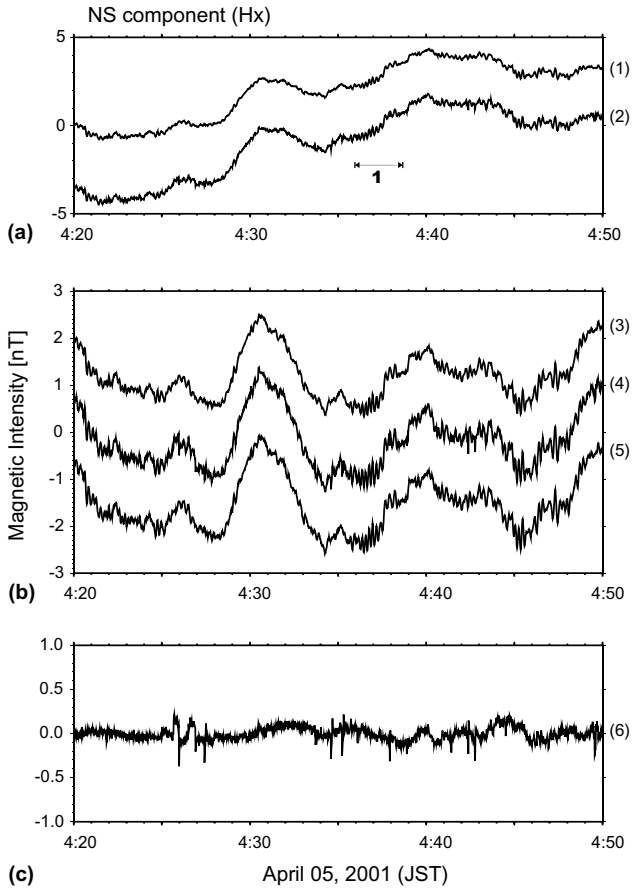

Fig. 6. Experimental results of the global signal reduction in NS component (H_x) at **KYS** station. (a) Original raw data at **KAK** and **KYS**. (b) Filtered and estimated external source field at **KYS** with the use of the ISTF approach. (c) The residual. The arrow (1) corresponds to the period when the geomagnetic pulsations turned up.

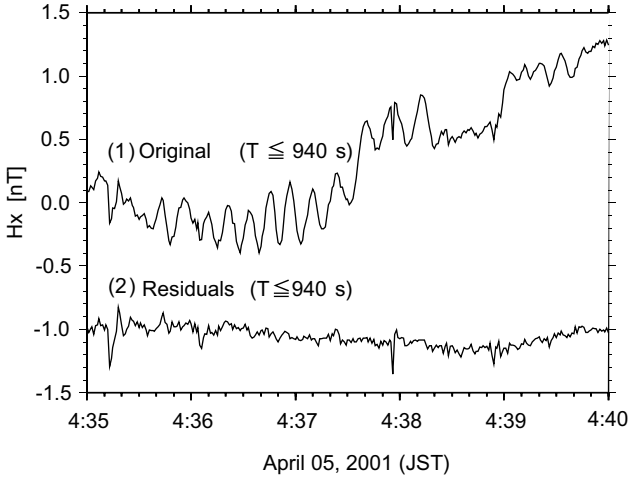

Fig. 7. The result of the reduction of geomagnetic pulsations ($T \approx 12.5$ s, NS component). (1) The high-pass filtered ($T \leqslant 940$ s) original data at **KYS**. (2) The residuals ($T \leqslant 940$ s). It is found that almost all of geomagnetic pulsations are eliminated satisfactorily.

ISTF approach. Therefore, the residual components must be local and regional variations observed at **KYS**, which actually turned up to be more visible.

In order to verify the effectiveness of the global signal reduction, we calculate the coherences of time series between **KAK** and array stations. Fig. 8 shows NS components of the squared coherences between **KAK** and **KYS** stations averaged over three hours in the period of 03:00–06:00 (JST) on April 5, 2001. The coherence of the original data (open circles) is high in the period of $T > 8$ s, and it has a maximum value at the period of the observed geomagnetic pulsations ($T \approx 12.5$ s). On the other hand, the coherences between original data at **KAK** and residuals at **KYS** (open squares) are reduced for the whole period of our concern. This implies that the coherent signals between these two stations (that is, global natural signals from the external sources) were eliminated satisfactorily.

Applying the same procedure to the EW and vertical components, the corresponding results are illustrated in Figs. 9 and 10. In the case of horizontal components, the amplitude of magnetic pulsation started at 04:35 is about 0.3–0.6 nT, as shown in Figs. 6(b) and 9(b). After adopting the present reduction method, the amplitude of estimated pulsation component is considerably reduced as shown in Figs. 6(c) and 9(c). As for the vertical components as shown in Fig. 10(a), original data at **KAK** (1) and **KYS** (2) are found to exhibit some phase differences. Roughly said, the estimated external source fields at **KYS** (5) are similar to the observed data (4), which implies that the phase differences between the two stations could be estimated through the ISTF. And it seems that the regional/local variation in vertical component is well estimated.

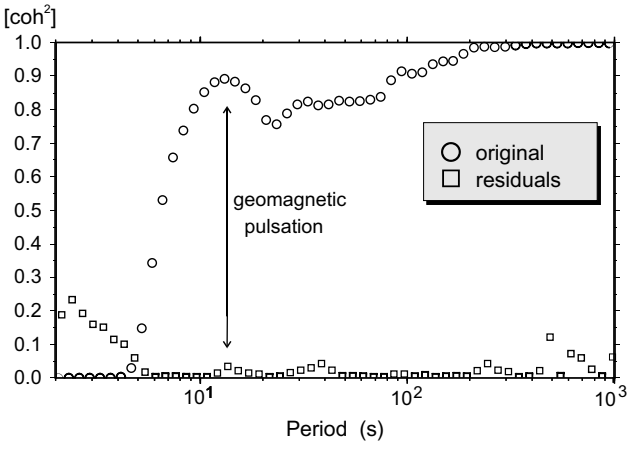

Fig. 8. The squared coherences of NS components between **KAK** and **KYS** stations averaged over 3 h in the period of 03:00–06:00 (JST) on April 5, 2001. Circles show the original coherences between **KAK** and **KYS**. Squares show the coherences between originals at **KAK** and residuals at **KYS**.

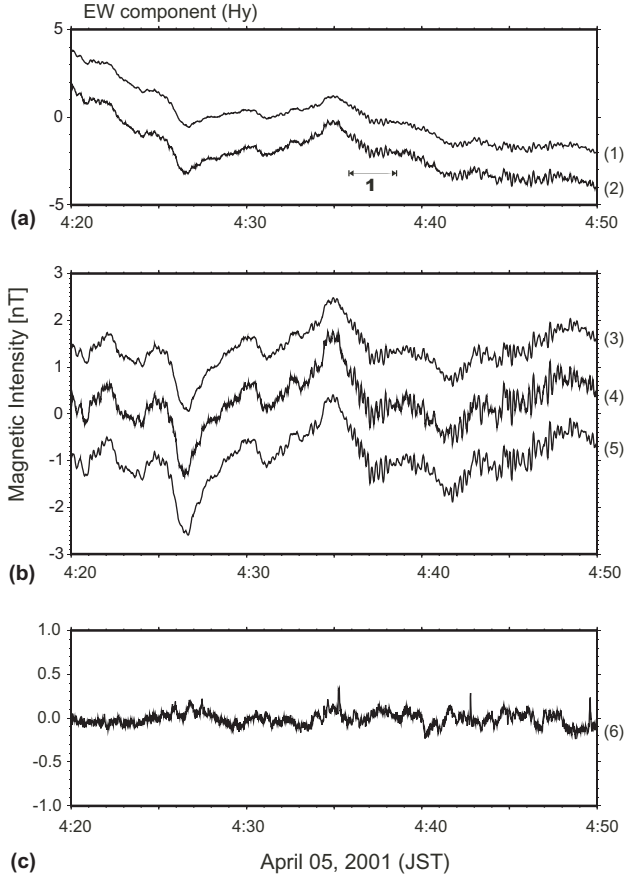

Fig. 9. Experimental results of the global signal reduction in EW component (H_y) at **KYS** station. (a) Original raw data at **KAK** and **KYS**. (b) Filtered and estimated external source field at **KYS** with the use of the ISTF approach. (c) The residual. The arrow (1) corresponds to the period when the geomagnetic pulsations turned up.

The results of NS component are shown in the following. Fig. 11 shows the results of global signal reduction with the use of ISTF approach. Fig. 11(a) indicates the filtered (high pass; period $T \leqslant 940$ s) original data (the upper line in each set) and the estimated external signals based on ISTF approach (the lower line in each set) at **UNB**, **UCU** and **KYS** stations. Fig. 11(b) is residuals at these three stations, and we can say that the trend is well removed. The selected time interval corresponds to the time when the first DC-driven train of the day started around the array stations. With respect to the timetable of the trains, the possible operations are indicated in Fig. 11(b). Fig. 12 shows locations of the passenger stations and the train based on the diagram. It is clearly seen that the transient signals are corresponding to the acceleration and deceleration of the nearby train.

Figs. 13 and 14 illustrate the superiority of the proposed method. Fig. 13 shows the results at **KYS** station based on Fourier transform of NS component with $T \leqslant 940$ s. The curves (1) and (2) in Fig. 13 indicate the

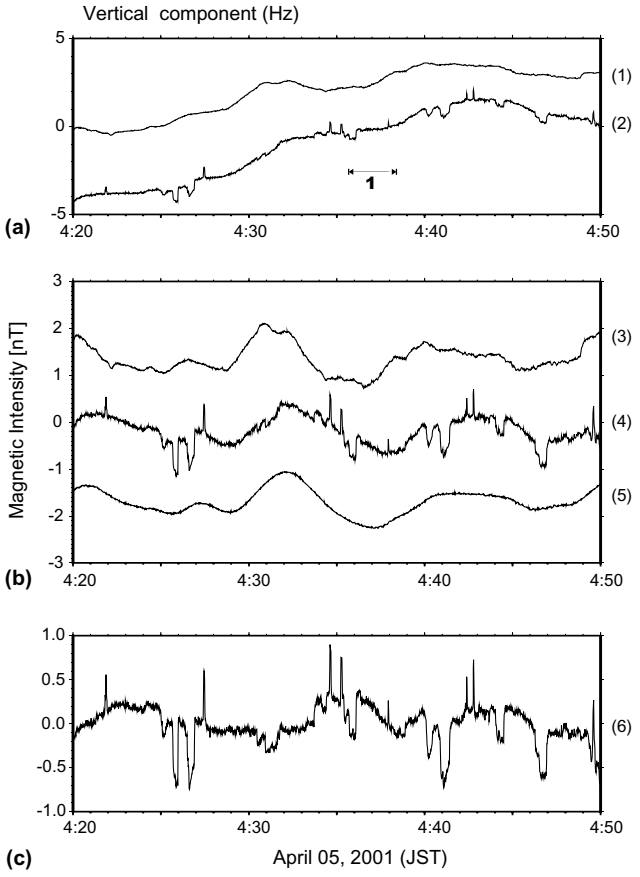

Fig. 10. Experimental results of the global signal reduction in vertical component (H_z) at **KYS** station. (a) Original raw data at **KAK** and **KYS**. (b) Filtered and estimated external source field at **KYS** with the use of the ISTF approach. (c) The residual. The arrow (1) corresponds to the period when the geomagnetic pulsations turned up.

high-pass filtered original data at **KAK** and **KYS**, respectively. The curve (3) in this figure is the estimated external signals at **KYS** based on the ISTF approach using the FFT approach. The trend variations in (2) and (3) is quite different, because of ill estimation of the ISTF. In general, Fourier transform is not robust for the contamination of transient signals. The curve (4) shows the residuals between the curves (2) and (3). On the other hand, high-pass filtered original data at **KAK** and **KYS** are very similar. Therefore, the residual of them is investigated both by Fourier and wavelet approaches. The results are summarized in Fig. 14, in which the curve (1) shows the residuals (NS component, $T \leqslant 940$ s) in the Fourier domain between original data at **KAK** and **KYS** ((1)–(2) in Fig. 13). The curve (2) is the residual computed in wavelet domain. The curve (3) indicates the residual obtained by the ISTF approach with wavelet transform (cf. Fig. 6(c) or 11(b)). We can see geomagnetic pulsations from external sources marked by an arrow (1) are removed effectively by using the ISTF. This figure indicates the advantage of

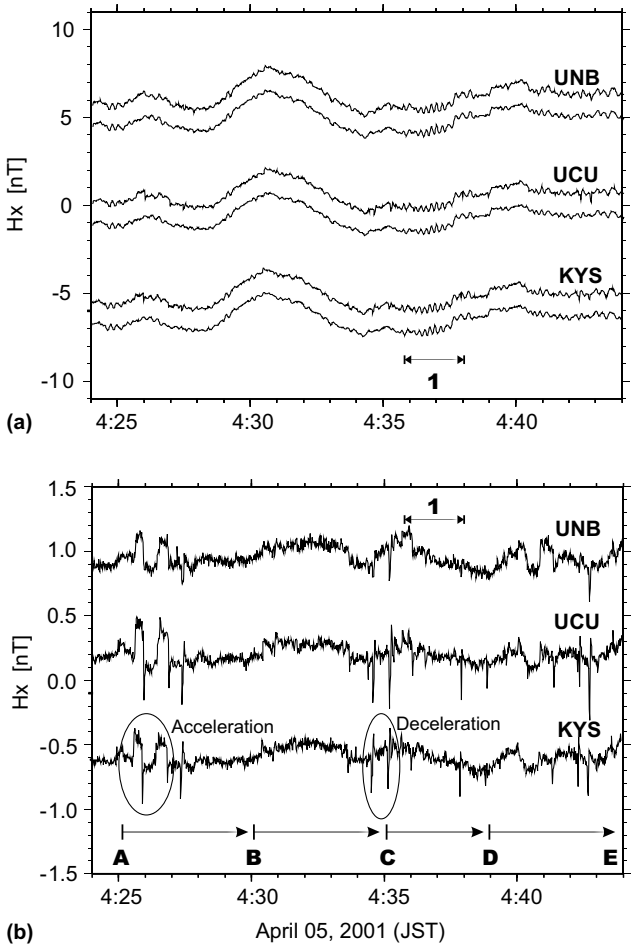

Fig. 11. The comparison of the global signal reduction among the array stations in Boso Peninsula (NS component, April 5, 2001). **KAK** is the remote reference station. **UNB**, **UCU** and **KYS** are target stations for estimating the ISTF. (a) The high-pass filtered original geomagnetic field variation (the upper line in each set, $T \leqslant 940$ s) and estimated external source field with the use of ISTF (the lower line in each set, $T \leqslant 940$ s). (b) The residuals between the upper and lower data in Fig. 11(a). The arrow (1) corresponds to the period when the geomagnetic pulsations turned up. The alphabetic indices in the figure correspond to the location of the passenger stations where the first train is running through (see Fig. 12).

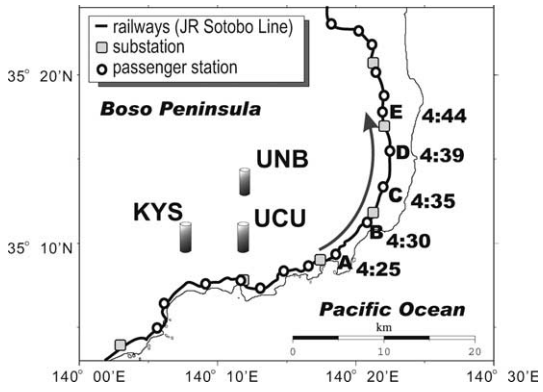

Fig. 12. Configuration map of railway stations and the location of the first train. The alphabetic indices correspond to the railway station in Fig. 11(b). The time is picked up from the diagram (departure time).

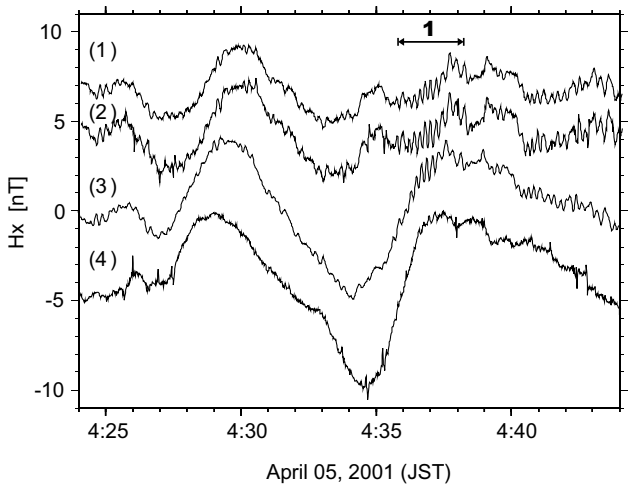

Fig. 13. The results of the ISTF approach with the use of Fourier transform (NS component, $T \leqslant 940$ s). The same time period was examined as in the case of the wavelet transform shown in Fig. 6. (1) and (2) indicate the high-pass filtered original data at **KAK** and **KYS**, respectively, which are corresponding to the curves (1) and (2) in Fig. 6(b); (3) indicates the estimated external source field at **KYS**, which is corresponding to the curve (4) in Fig. 6(b); (4) indicates the residuals between (2) and (3), which is corresponding to Fig. 6(c). The arrow (1) shows the active periods of geomagnetic pulsations.

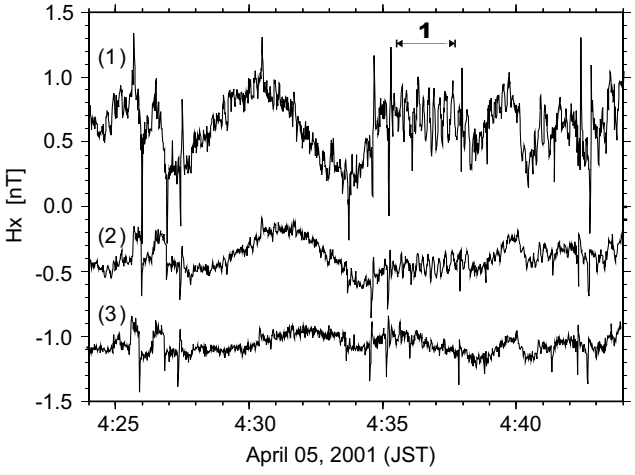

Fig. 14. The results of the differences between high-pass filtered original data at **KAK** and **KYS** (NS components, $T \leqslant 940$ s). (1) The result of the Fourier transform. (2) The result of the wavelet transform. (3) The residuals of the global signal reduction using ISTF approach with wavelet transform (cf. Fig. 6(c) or Fig. 11(b)). The arrow (1) shows the active periods of geomagnetic pulsations.

adopting wavelet transform, and further, it strongly suggests the effectiveness of our global noise reduction.

4. Discussion and conclusion

In order to study ULF geomagnetic field changes associated with earthquakes, it is important to discriminate the signals from noises such as magnetic pulsations originated from the external sources and artificial noises from DC-driven trains and factories. As the first step for this aim, the ISTF approach with the use of wavelet transform is proposed. The interstation transfer functions have information on relative underground electrical properties between the reference and a certain station. We applied the proposed method to data obtained from the ULF electromagnetic sensor array in the Boso Peninsula, Japan. The data from the Kakioka Magnetic Observatory were used as a remote reference. Results showed global geomagnetic variations such as geomagnetic pulsations can be removed successfully in the horizontal components. The proposed method has a capacity to eliminate the most intense global signals effectively and it is suggested to capture signals lying in the background.

This fact gives us an opportunity to improve the signal processing developed for the study of earthquake-related ULF magnetic variations; for example, principal component analysis of ULF geomagnetic data associated with large earthquakes (Gotoh et al., 2002; Uyeda et al., 2002). They analyzed the horizontal magnetic field data obtained from the closely spaced three stations with intersensor distance of about 5 km. Since they used three variables, it is possible to separate three principal components in principle. They indicated that the first principal component refers to the global magnetic variations such as geomagnetic pulsations and the second principal component to human activity. The weak earthquake-related signals might be included in the third principal component. If the proposed method is applied to the preprocessing of their approach, the most intense signal will be removed and more convincing result may be expected. It is interesting to apply the proposed method to other data which indicate the anomalous geomagnetic change associated with crustal activities.

The future tasks of the proposed method are as follows; (1) Investigate the objective estimation of the optimal interstation transfer functions (for example the robust estimation (Chave et al., 1987; Egbert, 1997)). (2) Develop the methodology to remove the regional artificial signal, especially DC driven train noises. After reduction of global signals from the external sources, it is clearly seen that the transient signals are corresponding to the acceleration and deceleration of the nearby train (see Fig. 9(b)). The amplitude of the signal depends on the geometry of the train and its sub-power stations. If we can find remarkable signal patterns or typical patterns, the automatic detection and discrimination could be available.

Acknowledgements

The authors wish to express their thanks to Japan Meteorological Agency for providing data of Kakioka

Magnetic Observatory. This work was partially supported by the JSPS Grants-in-Aid for Scientific Research #13650477.

References

Beamish, D., Banks, R.J., 1983. Geomagnetic variation anomalies in northern England: processing and presentation of data from a non-simultaneous array. Geophys. J. Roy. Astr. Soc. 75, 513–539.

Chave, A.D., Thomson, D.J., Ander, M.E., 1987. On the robust estimation of power spectra, coherences, and transfer functions. J. Geophys. Res. 92 (B1), 633–648.

Egbert, G.D., 1997. Robust multiple-station magnetotelluric data processing. Geophys. J. Int. 130, 475–496.

Farge, M., 1992. Wavelet transforms and their applications to turbulence. Ann. Rev. Fluid Mech. 24, 395–457.

Fraser-Smith, A.C., Bernardi, A., McGill, P.R., Ladd, M.E., Helliwell, R.A., Villard Jr, O.G., 1990. Low-frequency magnetic field measurements near the epicenter of the. Geophys. Res. Lett. 17, 1465–1468.

Fujiwara, S., Toh, H., 1996. Geomagnetic transfer functions in Japan obtained by first order geomagnetic survey. J. Geomagn. Geoelectr. 48, 1071–1101.

Gotoh, K., Akinaga, Y., Hayakawa, M., Hattori, K., 2002. Principal component analysis of ULF geomagnetic data for Izu islands earthquakes in July 2000. J. Atm. Electr. 22, 1–12.

Hattori, K., Akinaga, Y., Hayakawa, M., Yumoto, K., Nagao, T., Uyeda, S., 2002. ULF magnetic anomaly preceding the 1997 Kagoshima earthquakes. In: Hayakawa, M., Molchanov, O.A. (Eds.), Seismo Electromagnetics: Lithosphere–Atmosphere–Ionosphere Coupling. TERRAPUB, Tokyo, pp. 19–28.

Hayakawa, M. (Ed.), 1999. Atmospheric and Ionospheric Electromagnetic Phenomena Related with Earthquakes. Terra Scientific Publishing Company (TERRAPUB), Tokyo, p. 996.

Hayakawa, M., Fujinawa, Y. (Eds.), 1994. Electromagnetic phenomena related to earthquake prediction. Terra Scientific Publishing Company (TERRAPUB), Tokyo, p. 677.

Hayakawa, M., Molchanov, O.A. (Eds.), 2002. Seismo Electromagnetics: Lithosphere-Atmosphere-Ionosphere Coupling. Terra Scientific Publishing Company (TERRAPUB), Tokyo, p. 477.

Hayakawa, M., Itoh, T., Hattori, K., Yumoto, K., 2000. ULF electromagnetic precursors for an earthquake at Biak, Indonesia on February 17, 1996. Geophys. Res. Lett. 27, 1531–1534.

Hayakawa, M., Kawate, R., Molchanov, O.A., Yumoto, K., 1996. Results of ultra-low-frequency magnetic field measurements during the Guam earthquake of 8 August 1993. Geophys. Res. Lett. 23, 241–244.

Kawate, R., Molchanov, O.A., Hayakawa, M., 1998. Ultra-low-frequency magnetic fields during the Guam earthquake of 8 August 1993 and their interpretation. Phys. Earth Planet. Inter. 105, 229–238.

Kopytenko, Y.A., Matishvili, T.G., Voronov, P.M., Kopytenko, E.A., Molchanov, O.A., 1993. Detection of ultra-low-frequency emissions connected with the Spitak earthquake and its aftershock activity, based on geomagnetic pulsations data at Dusheti and Vardzia observatories. Phys. Earth Planet. Inter. 77, 85–95.

Molchanov, O.A., Hayakawa, M., 1995. Generation of ULF electromagnetic emissions by microfracturing. Geophys. Res. Lett. 22, 3091–3094.

Molchanov, O.A., Kopytenko, Y.A., Voronov, P.M., Kopytenko, E.A., Matiashvili, T.G., Fraser-Smith, A.C., Bernardi, A., 1992. Results of ULF magnetic field measurements near the epicenters of the Spitak (Ms = 6.9) and Loma Prieta (Ms = 7.1) earthquakes: comparative analysis. Geophys. Res. Lett. 19, 1495–1498.

Morlet, J., Arens, G., Fourgeau, E., Giard, D., 1982. Wave propagation and sampling theory—Part I: Complex signal and scattering in multilayered media. Geophysics 47, 203–221.

Rikitake, T., 1969. The undulation of an electrically conductive layer beneath the islands of Japan. Tectonophys 7, 257–264.

Schmucker, U., 1970. Anomalies of geomagnetic variations in the southwestern United States. Bull. Scripps Inst. Oceanogr. 13, 1–165.

Torrence, C., Compo, G.P., 1998. A practical guide to wavelet analysis. Bull. Am. Meteor. Soc. 79, 61–78.

Uyeda, S., Hayakawa, M., Nagao, T., Molchanov, O.A., Hattori, K., Orihara, Y., Gotoh, K., Akinaga, Y., Tanaka, H., 2002. Electric and magnetic phenomena observed before the volcano-seismic activity 2000 in the Izu islands region Japan. Proc. US Natl. Acad. Sci. 99, 7352–7355.

Vallianatos, F., Tzanis, A., 1999. A model for the generation of precursory electric and magnetic fields associated with the deformation rate of the earthquake focus. In: Hayakawa, M. (Ed.), Atmospheric and Ionospheric Electromagnetic Phenomena Related with Earthquakes. TERRAPUB, Tokyo, pp. 287–305.